

# Preparation and characterization of surfactant-modified hydroxyapatite/zeolite composite and its adsorption behavior toward humic acid and copper(II)

Yanhui Zhan · Jianwei Lin · Jia Li

Received: 28 June 2012 / Accepted: 22 August 2012 / Published online: 8 September 2012  
© Springer-Verlag 2012

**Abstract** A novel composite material, i.e., surfactant-modified hydroxyapatite/zeolite composite, was used as an adsorbent to remove humic acid (HA) and copper(II) from aqueous solution. Hydroxyapatite/zeolite composite (HZC) and surfactant-modified HZC (SMHZC) were prepared and characterized by X-ray diffraction, Fourier transform infrared spectroscopy, and field emission scanning electron microscope. The adsorption of HA and copper(II) on SMHZC was investigated. For comparison purposes, HA adsorption onto HZC was also investigated. SMHZC exhibited much higher HA adsorption capacity than HZC. The HA adsorption capacity for SMHZC decreased slightly with increasing pH from 3 to 8 but decreased significantly with increasing pH from 8 to 12. The copper(II) adsorption capacity for SMHZC increased with increasing pH from 3 to 6.5. The adsorption kinetic data of HA and copper(II) on SMHZC obeyed a pseudo-second-order kinetic model. The adsorption of HA and copper(II) on SMHZC took place in three different stages: fast external surface adsorption, gradual adsorption controlled by both film and intra-particle diffusions, and final equilibrium stage. The equilibrium adsorption data of HA on SMHZC better fitted to the Langmuir isotherm model than the Freundlich isotherm model. The equilibrium adsorption data of copper(II) on SMHZC could be described by the Langmuir, Freundlich, and Dubinin–Radushkevich isotherm models. The presence of copper(II) in solution enhanced HA adsorption onto SMHZC. The presence of HA in solution enhanced copper(II) adsorption onto SMHZC. The mechanisms for the adsorption of HA on

SMHZC at pH 7 may include electrostatic attraction, organic partitioning, hydrogen bonding, and Lewis acid–base interaction. The mechanisms for the adsorption of copper (II) on SMHZC at pH 6 may include surface complexation, ion exchange, and dissolution–precipitation. The obtained results indicate that SMHZC can be used as an effective adsorbent to simultaneously remove HA and copper(II) from water.

**Keywords** Surfactant-modified hydroxyapatite/zeolite composite · Humic acid · Copper(II) · Adsorption

## Introduction

The contamination of surface and ground waters caused by toxic heavy metal ions has become a serious environmental issue because these ions are virtually non-biodegradable and tend to accumulate in living organisms, causing severe disorders and diseases (Lee et al. 2012; Tong et al. 2011; Yadav et al. 2012). Therefore, it is very important to remove heavy metal ions from contaminated water in terms of protecting human health and environment. There are several physico-chemical methods available for heavy metal ions removal from aqueous solution, including chemical precipitation, reverse osmosis, filtration, solvent extraction, electrodeposition, electrodialysis, ion exchange and adsorption, etc. (Da’na and Sayari 2011; Engates and Shipley 2011; Sulaymon et al. 2012; Tong et al. 2011; Wang et al. 2011a; Wu et al. 2012). Among these methods, adsorption is considered as an effective method for heavy metal ions removal from aqueous solution due to its cost effectiveness and high efficiency (Lee et al. 2012; Wang et al. 2011a).

Humic acid (HA), commonly present in natural waters and soils, is an important component of natural organic matter (NOM) due to biological decomposition of organic

Responsible editor: Philippe Garrigues

Y. Zhan · J. Lin (✉) · J. Li  
College of Marine Science, Shanghai Ocean University,  
No.999 Hucheng Huan Road, Pudong District,  
201306, Shanghai, China  
e-mail: jwlin@shou.edu.cn

matter from plants and other organisms (Wang et al. 2011b, c). HA contains both hydrophobic and hydrophilic components as well as many chemical functional groups such as carboxylic, phenolic, carbonyl, and hydroxyl groups (Maghsoodloo et al. 2011). The presence of HA in water is not directly toxic but may cause some problems in drinking water production (Jarvis and Majewski 2012). For example, HA can react with chlorine during water treatment and produce carcinogenic disinfection by-products such as trihalomethanes (Imyim and Prapalimrunsi 2010; Jarvis and Majewski 2012). In addition, HA may cause water to have undesirable color and taste and bind heavy metals and other organic matter to increase their concentrations in water (Wang et al. 2011b). Therefore, it is very important to eliminate HA from water. Various methods such as chemical coagulation, membrane separation, advanced oxidation, ion exchange and adsorption, etc. have been developed to remove HA from aqueous solution (Hartono et al. 2009; Maghsoodloo et al. 2011; Wang et al. 2011b). Among these methods, adsorption is considered as an effective method for HA removal from aqueous solution due to its simplicity and high efficiency (Wang et al. 2011b).

Heavy metal ion in natural waters often coexists with NOM such as HA. When heavy metal ion is concurrently present with HA in water, their simultaneous removal is of crucial importance to simplify treatment processes and to reduce cost as much as possible. Activated carbon is a very popular adsorbent for removing contaminants from water due to its highly developed porosity, large surface area, variable characteristics of surface chemistry, and high degree of surface reactivity (Bouhamed et al. 2012; Jarvis and Majewski 2012), and it can simultaneously adsorb heavy metal ion and HA (Chen and Wu 2004). The adsorption properties of heavy metal ion and HA from single- and binary-component aqueous solutions on activated carbon have been extensively investigated in previous literatures (Bouhamed et al. 2012; Chen and Wu 2004; Daifullah et al. 2004; Demirbas et al. 2009; Rauthula and Srivastava 2011; Terdkiatburana et al. 2008; Wang et al. 2011a). However, activated carbon is not very effective in removal of large molecules such as HA because its micropores are inaccessible for HA molecules (Jarvis and Majewski 2012; Moussavi et al. 2011; Stárek et al. 1994; Tang et al. 2012). Therefore, efforts are still needed to exploit new and more effective adsorbents for simultaneous removal of heavy metal ion and HA from aqueous solution.

Zeolites are crystalline-hydrated aluminosilicates minerals characterized by cage-like structure with high internal and external surface areas (Neupane and Donahoe 2012). The use of zeolite as an efficient adsorbent to remove heavy metal cations from aqueous solution has gained great attention in recent years due to its high cation adsorption capacity and low cost (Jamil et al. 2010; Motsi et al. 2009, 2011;

Šljivić et al. 2009a; Wang and Ariyanto 2007). However, zeolite has a low adsorption capacity for HA in aqueous solution (Li et al. 2011; Zhan et al. 2010). Hydroxyapatite (HAP),  $\text{Ca}_{10}(\text{PO}_4)_6(\text{OH})_2$ , is a main mineral constituent of teeth, bones, and phosphate mineral rocks and has been proven to be a very efficient adsorbent for heavy metal cations removal from aqueous solution (Corami et al. 2007, 2008; Elkady et al. 2011; Hasret et al. 2012; Meski et al. 2011; Smičiklas et al. 2006; Wang et al. 2009; Zhu et al. 2008). Considering that HAP can be used an efficient adsorbent for removing phenol and low molecular weight organic acids that contain carboxylic group (such as acetic, oxalic, malic, and citric acids) from aqueous solution (Bouyarmene et al. 2010; Tanaka et al. 1997; Wei et al. 2011), HAP is expected to have a good affinity for HA in aqueous solution because HA contains phenolic and carboxylic groups. According to above introduction, HAP/zeolite composite (HZC) may be a potential adsorbent for simultaneous removal of heavy metal cation and HA from aqueous solution because HZC may be characteristics of both HAP and zeolite.

Zeolites possess net permanent negative charges on their framework surfaces resulting from isomorphic substitution of  $\text{Si}^{4+}$  by  $\text{Al}^{3+}$ , making them suitable for surface modification using cationic surfactants such as hexadecyltrimethylammonium bromide (HTAB) and cetylpyridinium bromide (CPB) in which each molecule is composed of a hydrophilic and positively charged head group and a hydrophobic tail (Chao and Chen 2012; Guan et al. 2010; Zhan et al. 2010). This surfactant-modified zeolite (SMZ) has been proven to exhibit a good adsorption capacity for HA in aqueous solution (Li et al. 2011; Zhan et al. 2010). In addition, since loading of cationic surfactant with large molecular weight (e.g., HTAB and CPB) onto zeolites is only limited to these external cation exchange sites, SMZ is also capable of adsorbing heavy metal cations from aqueous solution (Chao and Chen 2012; Neupane and Donahoe 2012). These results indicate that surface modification of HZC with cationic surfactant is expected to enhance its HA adsorption capacity, and this surfactant-modified HZC (SMHZC) may be a potential adsorbent for simultaneous removal of heavy metal cation and HA from aqueous solution. However, to the best of our knowledge, studies investigating the adsorption of heavy metal cation and HA on SMHZC have never been reported.

In this study, HZC and SMHZC were prepared and characterized by X-ray diffraction (XRD), Fourier transform infrared (FTIR) spectroscopy, and field emission scanning electron microscope (FE-SEM). The adsorption of HA and copper(II) on SMHZC was investigated by using batch experiments. For comparison purposes, HA adsorption onto HZC was also investigated by using batch experiments.

## Materials and methods

### Materials

Natural zeolite was collected from a mineral deposit in Jinyun County, Zhejiang Province, China and ground and sieved to obtain the geometric size less than 0.075 mm. Cationic surfactant CPB with minimum 99 % active substance was supplied from Sinopharm Chemical Reagent Co. Ltd., China and used without further purification. HA was supplied from Aldrich Chemical Co. and used without further purification. Analytical-grade  $\text{Cu}(\text{NO}_3)_2 \cdot 3\text{H}_2\text{O}$ ,  $\text{Ca}(\text{NO}_3)_2 \cdot 4\text{H}_2\text{O}$ ,  $(\text{NH}_4)_2\text{HPO}_4$ ,  $\text{NH}_3 \cdot \text{H}_2\text{O}$ ,  $\text{NaCl}$ ,  $\text{NaOH}$ , and  $\text{HCl}$  were supplied from Sinopharm Chemical Reagent Co. Ltd., China.

### Preparation of HZC

First,  $\text{Ca}(\text{NO}_3)_2 \cdot 4\text{H}_2\text{O}$  was dissolved in distilled water to form 100 mL of 2 mol/L solution, into which 20 g of natural zeolite was added and 2 mol/L  $(\text{NH}_4)_2\text{HPO}_4$  solution was also added with a Ca/P molar ratio of 1.667. The suspension solution was then buffered to pH=9 using  $\text{NH}_3 \cdot \text{H}_2\text{O}$  solution. After 72 h of shaking, the solid was collected by centrifugation and repeatedly washed with distilled water until neutral. Then, the solid was treated with 400 mL of 1 mol/L  $\text{NaCl}$  solutions at a constant shaking speed of 150 rpm for 24 h. After that, the solid was collected by centrifugation, repeatedly washed with distilled water until no  $\text{Cl}^-$  was detected by  $\text{AgNO}_3$  solution, and dried in an oven at 378 K for 24 h. Finally, the dried solid was ground and sieved to obtain the geometric size less than 0.1 mm.

### Preparation of SMHZC

First, 10 g of the previously prepared HZC was added into 150 mL of 25 mmol/L CPB solution. The mixture was then placed in a thermostatic water bath shaker at a constant shaking speed of 150 rpm for 24 h, with the temperature maintained at 313 K. The solid was then collected by centrifugation and washed with distilled water repeatedly in order to remove superficially held CPB molecules. The residual CPB concentration in the supernatant was determined using a TU-1901 UV/Vis spectrophotometer (Beijing Purkinje General Instrument Co., Ltd., China) at 259 nm. Finally, the solid was dried in an oven at 323 K for 24 h.

### Characterization of adsorbent materials

FTIR spectra of natural zeolite, HZC, and SMHZC were recorded on a Nicolet 5700 model FTIR spectrometer (Thermo Nicolet Corporation, USA) at 400–4,000  $\text{cm}^{-1}$ . The identification of crystalline phase was performed using

an X'Pert PRO X-ray diffractometer with  $\text{Cu K}\alpha$  radiation (PANalytical, the Netherlands) operating at 40 kV and 40 mA. The surface morphologies of natural zeolite, HZC, and SMHZC were observed by a JSM-7500F FE-SEM (JEOL Ltd., Japan).

### Adsorption studies

The adsorption of HA and Cu(II) from single- and binary-component aqueous solutions was studied in batch mode. The batch adsorption experiments were performed in conical flasks containing a definite dosage of adsorbent and a given volume of adsorbate solution. The initial pH of adsorbate solution was adjusted to a definite value using 0.1 mol/L  $\text{NaOH}$  and 0.1 mol/L  $\text{HCl}$  solutions. The mixtures were then shaken at 150 rpm in a thermostatic water bath shaker at given temperature. After pre-defined contact time, the adsorbent was removed from the mixture by centrifugation. Then, the residual concentration of HA in the supernatant was analyzed using a TU-1901 UV/Vis spectrophotometer (Beijing Purkinje General Instrument Co., Ltd., China) at 259 nm, and the residual concentration of Cu(II) in the supernatant was analyzed using a TAS-990 atomic absorption spectrophotometer (Beijing Purkinje General Instrument Co., Ltd., China). The amount of adsorbate adsorbed on adsorbent at any time  $t$  ( $q_t$ , in milligrams per gram) was calculated according to the following equation:

$$q_t = \frac{(C_0 - C_t)V}{m} \quad (1)$$

where  $C_0$  is the initial concentration of adsorbate in solution (in milligrams per liter),  $C_t$  is the concentration of adsorbate in solution at any time  $t$  (in milligrams per liter),  $V$  is the volume of adsorbate solution (in liter), and  $m$  is the mass of adsorbent (in grams). The removal efficiency of adsorbate (in percent) was calculated according to the following equation:

$$\text{Removal efficiency(\%)} = \frac{C_0 - C_t}{C_0} \times 100 \quad (2)$$

## Results and discussion

### Characterization of adsorbent materials

The XRD patterns of natural zeolite, HZC, and SMHZC are shown in Fig. 1. The XRD pattern of the natural zeolite showed the characteristic peaks of clinoptilolite, mordenite, and quartz, indicating the presence of these minerals in the natural zeolite. The main XRD peaks at  $2\theta=9.94^\circ$ ,  $20.9^\circ$ ,  $22.4^\circ$ ,  $25.7^\circ$ ,  $26.7^\circ$ ,  $27.8^\circ$ , and  $50.2^\circ$ , which were in agreement with the characteristic XRD peaks of the natural zeolite, were observed in the HZC. This indicates the presence of the natural zeolite in the HZC. In addition, a comparatively broad

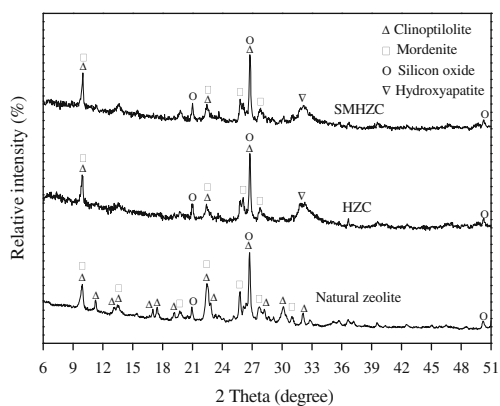


**Fig. 1** XRD patterns of natural zeolite, HZC, and SMHZe

diffraction peak at about  $2\theta=31.8^\circ$ , which was a characteristic XRD peak of HAP, was observed in the HZC. This indicates the presence of HAP in the HZC. The positions of the main XRD peaks of SMHZe were similar to those of HZC. This indicates that the modification of HZC with CPB does not lead to the significant structural change of HZC.

The FTIR spectra of natural zeolite, HZC, and SMHZe are shown in Fig. 2. The positions of the main adsorption bands for the natural zeolite were listed as follows: 3,627, 3,450, 1,644, 1,041, 796, and 466  $\text{cm}^{-1}$ . The bands at 3,627, 3,450, and 1,644  $\text{cm}^{-1}$  are attributed to the presence of zeolitic water (Elaiopoulos et al. 2010). The band at 1,041  $\text{cm}^{-1}$  is attributed to a strong T–O stretching vibration (Elaiopoulos et al. 2010). The band at 796  $\text{cm}^{-1}$  is attributed to quartz or amorphous  $\text{SiO}_2$  stretching vibration (Elaiopoulos et al. 2010). The band at 466  $\text{cm}^{-1}$  is attributed to Si–O–Si bending mode (Elaiopoulos et al. 2010). The positions of the main adsorption bands for the HZC were listed as follows: 3,442, 1,641, 1,035, 796, 604, 565, and 468  $\text{cm}^{-1}$ . The bands at 3,442 and 1,641  $\text{cm}^{-1}$  are attributed to the OH stretching and bending vibrations, respectively (Shaltout et al. 2011). The band at 1,035  $\text{cm}^{-1}$  is attributed to the strong T–O stretching vibration and the bending vibration ( $\nu_3$ ) of the phosphate group of HAP (Elaiopoulos

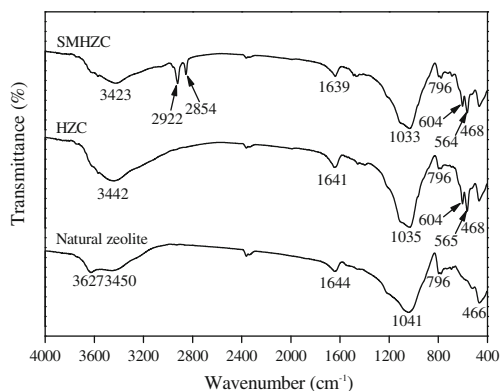


**Fig. 2** FTIR spectra of natural zeolite, HZC, and SMHZe

et al. 2010; Suresh Kumar et al. 2010). The band at 796  $\text{cm}^{-1}$  is attributed to quartz or amorphous  $\text{SiO}_2$  stretching vibration (Elaiopoulos et al. 2010). The bands at 604 and 565  $\text{cm}^{-1}$  are attributed to the bending vibration ( $\nu_4$ ) of the phosphate group of HAP (Suresh Kumar et al. 2010). The band at 468  $\text{cm}^{-1}$  is attributed to Si–O–Si bending mode (Elaiopoulos et al. 2010). It was obvious that the FTIR spectrum of HZC showed the combination of characteristic adsorption bands due to the groups of the natural zeolite and HAP, indicating the presence of the natural zeolite and HAP in the HZC. The FTIR spectrum of SMHZe showed two pronounced adsorption bands at 2,854 and 2,922  $\text{cm}^{-1}$ , which are attributed to the symmetric and asymmetric – $\text{CH}_2$  stretching vibrations, respectively (Zhan et al. 2010). The presence of bands at 2,854 and 2,922  $\text{cm}^{-1}$  in the SMHZe spectrum, which were absent in the HZC spectrum, indicates that CPB molecules have been loaded onto the surface of HZC after the contact of HZC with CPB solution.

The surface morphologies of natural zeolite, HZC, and SMHZe were determined by using a FE-SEM. The obtained results are given in Fig. 3. As shown in Fig. 3a, the natural zeolite was characterized by a drusy texture with very high microporosity, partially developed crystalline laminar habits and conglomerates of compact crystals. The surface morphologies of HZC and SMHZe were significantly different to that of the natural zeolite. When the surface of the natural zeolite was covered by agglomerated HAP particles, the zeolite crystals could not be seen clearly (Fig. 3b). When the surface of the natural zeolite was covered by agglomerated HAP particles and CPB molecules, the zeolite crystals also could not be seen clearly (Fig. 3c). The HZC and SMHZe had a porous and coarse surface texture, which possibly indicates that these solid materials are highly porous with a high adsorption capacity for pollutant.

According to the difference between the initial concentration of CPB in the solution and the residual concentration of CPB in the solution after the modification of HZC with CPB, the amount of CPB loaded onto HZC was found to be 235 mmol/kg. As HAP had a very low affinity toward CPB in aqueous solution (data not shown), the loaded CPB molecules on the HZC mainly formed CPB layers on the external surface of the zeolite. When aqueous cationic surfactant concentrations are larger than the critical micelle concentration and sufficient surfactant is present in solution, the loaded cationic surfactant molecules primarily form a bilayer on the zeolite surface with the lower layer held by electrostatic attraction, while the upper layer is bound to the lower layer by hydrophobic interaction (Li et al. 2000; Malekian et al. 2011; Zhan et al. 2010). As the amount of CPB available for the modification of HZC was much higher than that of CPB loaded on HZC, the loaded CPB molecules on the HZC mainly formed CPB bilayers on the external surface of the zeolite.



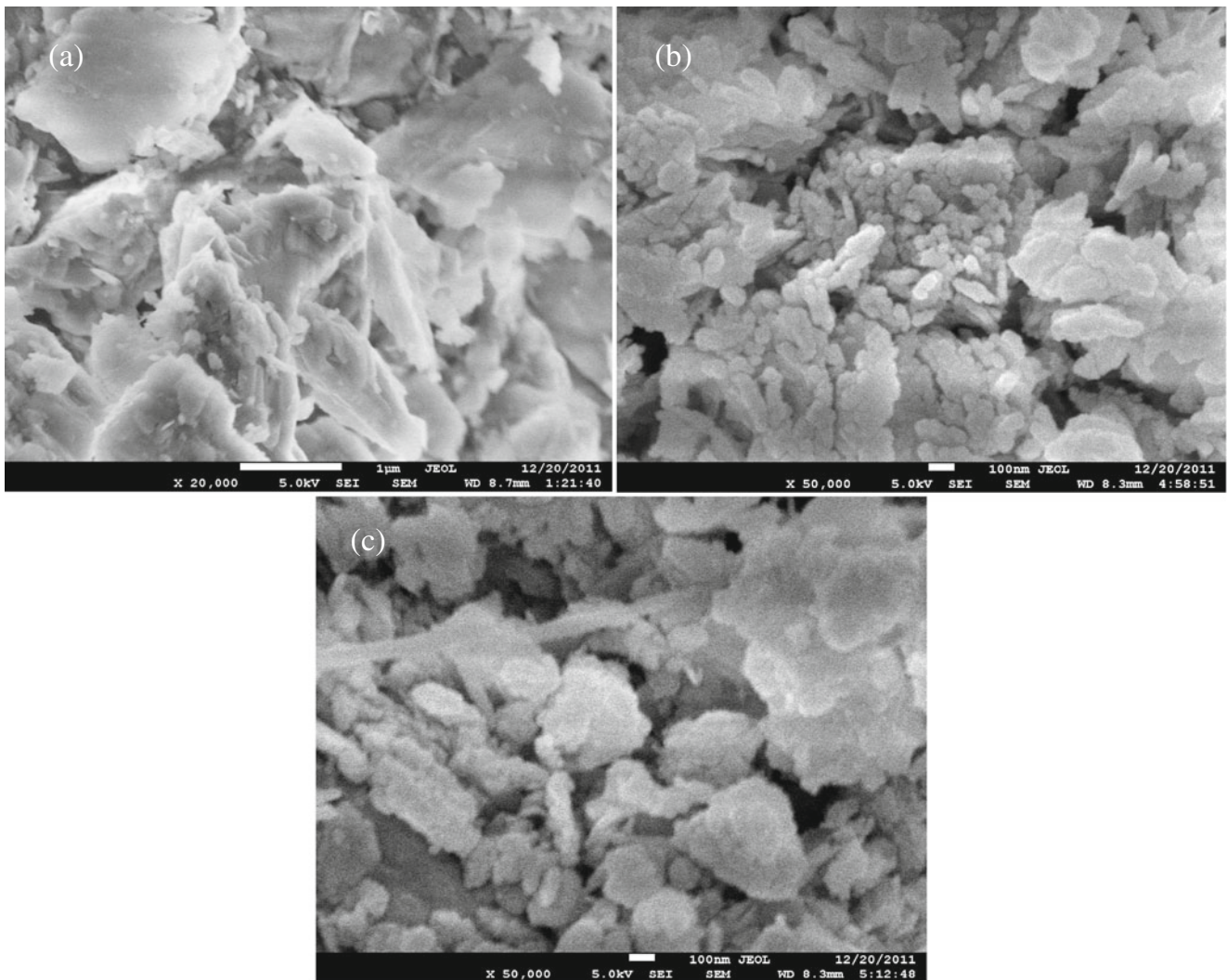


**Fig. 3** SEM images of **a** natural zeolite, **b** HZC, and **c** SMHZC

### Adsorption of HA on HZC and SMHZC

#### *Effect of adsorbent dosage on HA adsorption onto HZC and SMHZC*

The adsorption of HA on HZC and SMHZC as a function of adsorbent dosage is shown in Fig. 4. Figure 4 showed that the HA removal efficiency of HZC increased from 17 to 78 % with the increase of adsorbent dosage from 0.2 to 3 g/L, and the HA removal efficiency of SMHZC increased from 48 to 95 % with the increase of adsorbent dosage from 0.2 to 0.8 g/L. With a further increase in the dosage of SMHZC to 3 g/L, the HA removal efficiency slightly went up to 97 %. The increase of the HA removal efficiency with increasing adsorbent dosage was attributed to the increase in the adsorbent concentration, which increased the available surface area and adsorption sites (Wen et al. 2012). However, the amounts of HA adsorbed on HZC and

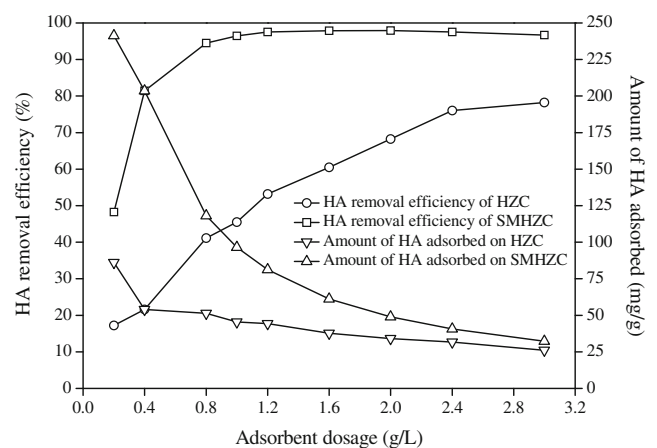


**Fig. 4** Effect of adsorbent dosage on HA adsorption onto HZC and SMHZC (solution volume 50 mL; initial HA concentration 100 mg/L; pH 7; contact time 24 h; temperature 303 K)

SMHZC decreased significantly with the increase of adsorbent dosage from 0.2 to 3 g/L. This was attributed to the unsaturation of adsorption sites during the adsorption process (Wen et al. 2012). Figure 4 also showed that SMHZC exhibited a much higher adsorption capacity for HA than HZC, indicating that the surface modification of HZC with CPB significantly enhances its HA adsorption capacity and thus SMHZC is more suitable as an efficient adsorbent for removing HA from aqueous solution than HZC.

*Effect of solution pH on HA adsorption onto HZC and SMHZC*

The adsorption of HA on HZC and SMHZC as a function of solution pH is shown in Fig. 5. As shown in Fig. 5, the HA adsorption capacity for HZC increased slightly with increasing initial pH from 3 to 5 but decreased continuously with increasing initial pH from 5 to 12. HA contains a variety of weakly acidic functional groups such as carboxylic and phenolic groups (Tao et al. 2010). The  $pK_a$  values of carboxylic and phenolic groups are around 3 and 9 (Tao et al. 2010); thus, HA is expected to be negatively charged by the deprotonation of carboxylic groups at pH above 3. The HA adsorption capacity for HZC is mainly related to the surface properties of HAP because the natural zeolite has negligible affinity toward HA in aqueous solution (Zhan et al. 2010). The HAP surface charge is expected to be the result of acid–base interactions of the reactive surface sites (Bouyarmane et al. 2010; Wu et al. 1991). The  $pH_{PZC}$  (pH at the point of zero charge) of pure HAP was determined by using the procedure described in the previous literatures (Balistrieri and Murray 1981; Smičiklas et al. 2000), and it was found to be 7.1. Below the  $pH_{PZC}$  of HAP, protons in the solution are consumed by the protonation of the surface  $\equiv P-O^-$  and  $\equiv Ca-OH$  groups, resulting in the increase of final pH value (Smičiklas et al. 2006). The positively charged  $\equiv Ca-OH_2^+$  and neutral  $\equiv P-OH$  groups prevail on the HAP surface in

solutions at pH below the  $pH_{PZC}$  of HAP, making surface charge of HAP in this pH region positive (Smičiklas et al. 2006). In this case, the adsorption of HA on HZC may be achieved through the electrostatic attraction between the negatively charged HA molecules and the positively charged HAP surfaces. In addition, the oxygen atom of functional groups of HA may interact with  $Ca^{2+}$  groups of HAP via Lewis acid–base interaction (Bouyarmane et al. 2010). The adsorption of HA on HZC at pH below the  $pH_{PZC}$  of HAP may also be achieved through hydrogen bonding. For example, the  $\equiv P-OH$  groups on the HAP surface and the carboxylic groups of HA molecules may form hydrogen bonding (Wei et al. 2011). With the increase of initial pH from 3 to 5, the ionization of carboxyl groups of HA molecules increases and more negatively charged carboxyl groups exist in HA molecules. This will result in the increase of the electrostatic force between the negatively charged HA molecules and the positively charged HAP surfaces, which may cause an increased HA adsorption capacity. With the increase of initial pH from 5 to the  $pH_{PZC}$  of HAP, the positive charge on the HAP surface decreases. Hence, less negatively charged HA molecules will be attracted to the HAP surface, which may cause a decreased HA adsorption capacity. Above the  $pH_{PZC}$  of HAP, final pH value decrease occurs due to the consumption of  $OH^-$  via the deprotonation of the surface  $\equiv Ca-OH_2^+$  and  $\equiv P-OH$  groups, and thus, neutral  $\equiv Ca-OH$  and negatively charged  $\equiv P-O^-$  groups predominate, causing HAP surface to become negatively charged in this pH region (Smičiklas et al. 2006). In this case, the electrostatic attraction between HA molecules and HAP surfaces is impossible. The adsorption of HA on HZC at pH above the  $pH_{PZC}$  of HAP may be attributed to the Lewis acid–base interaction between the oxygen atom of functional groups of HA and the  $Ca^{2+}$  groups of HAP. In addition, the adsorption of HA on HZC at pH above the  $pH_{PZC}$  of HAP may also be achieved through hydrogen bonding. For example, the  $P-O^-$  groups on the HAP surface and the phenolic hydroxyl groups of HA molecules may form hydrogen bonding (Bouyarmane et al. 2010). The increase of initial pH from the  $pH_{PZC}$  of HAP to 12 resulted in the increase of the electrostatic repulsion between the negatively charged HA molecules and the negatively charged HAP surfaces, which may reduce the HA adsorption capacity. It has been suggested that HA may exist in a spherical structure at lower pH value but exist in a rather linear or stretched structure at higher pH value (Maghsoodloo et al. 2011). This will cause less amount of HA adsorbed in the adsorbent pores at higher pH value. Therefore, the increase of the sizes of HA macromolecules with increasing pH may be another factor contributing the decrease of the adsorption capacity with increasing initial pH from 5 to 12.

As shown in Fig. 5, the HA adsorption capacity for SMHZC decreased slightly with increasing initial pH from 3 to 8 but decreased significantly with increasing initial pH

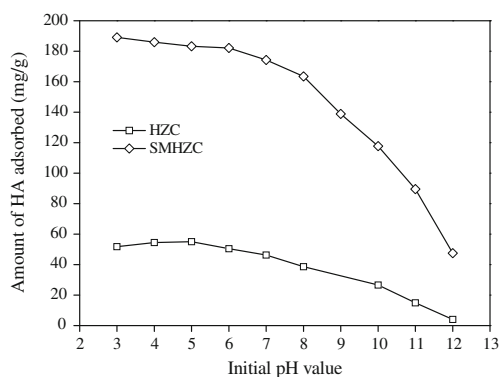


**Fig. 5** Effect of solution pH on HA adsorption onto HZC and SMHZC (solution volume 50 mL; initial HA concentration, 50 mg/L for HZC and 100 mg/L for SMHZC; adsorbent dosage 0.5 g/L; contact time 24 h; temperature 303 K)

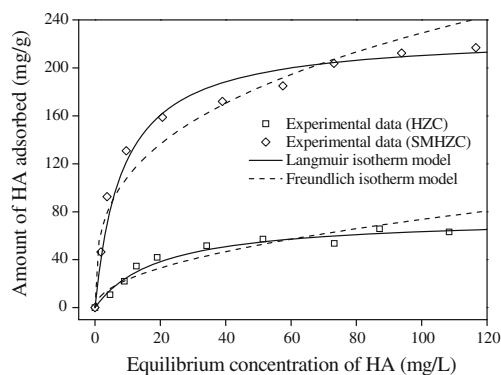


**Fig. 6** Adsorption isotherm of HA on HZC and SMHZC (solution volume 50 mL; pH 7; adsorbent dosage 0.5 g/L; contact time 24 h; temperature 303 K)

from 8 to 12. The HA adsorption capacity for SMHZC is not only related to the surface properties of HAP but also related to the loaded CPB molecules on the zeolite surface. At pH below the  $pH_{PZC}$  of HAP, the HA molecules in solution may interact with the HAP in SMHZC via electrostatic attraction, Lewis acid–base interaction, and hydrogen bonding. At pH above the  $pH_{PZC}$  of HAP, the HA molecules in solution may interact with the HAP in SMHZC via Lewis acid–base interaction and hydrogen bonding. The great difference of the HA adsorption capacities between HZC and SMHZC (Fig. 4) proves that the loaded CPB molecules on the HZC surface play a very important role in the adsorption process. Regarding the SMHZC, the loaded CPB molecules formed bilayers on the zeolite surface. This bilayer formation results in a charge reversal on the zeolite external surface from negative to positive and the positively charged outward-pointing head groups of CPB bilayers are balanced by counterion bromide (Li et al. 2000; Zhan et al. 2010). Therefore, the CPB bilayers on the zeolite surface may remove the negatively charged HA molecules from aqueous solution through anion exchange and electrostatic attraction (Li et al. 2011). In addition, a large number of hydrogen bonds between nitrogen of CPB bilayers and carboxylic groups and phenolic groups of HA molecules may additionally guarantee the effective adsorption of HA on SMHZC (Wang et al. 2006). The adsorption of HA on SMHZC may also involve partitioning of HA molecules into CPB bilayers (Ding and Shang 2010). At lower pH value, more of weakly acidic functional groups such as carboxylic and phenolic groups of HA molecules are in an uncharged state (Douliua et al. 2009) and more adsorbable due to the hydrogen bonding and organic partitioning. At higher pH value, more of these weakly acidic groups of HA molecules are ionized to exhibit anionic properties. The increase of initial pH from 3 to 8 results in the decrease of the hydrogen bonding and organic partitioning between HA molecules and CPB bilayers as well as the increase of the sizes of HA macromolecules, which are unfavorable for HA adsorption.

However, the increase of initial pH from 3 to 8 results in the increase of the electrostatic attraction between HA molecules and CPB bilayers, which is favorable for HA adsorption. The former may be partially counteracted by the latter, resulting in that the amount of HA adsorbed on SMHZC decreases slightly with increasing initial pH from 3 to 8. The increase of initial pH from 8 to 12 leads to the decrease of the hydrogen bonding and organic partitioning between HA molecules and CPB bilayers, the increase of the sizes of HA macromolecules, the increase of the competition between the hydroxyl ion and the negatively charged HA molecules for the same adsorption sites on the positively charged CPB bilayers, and the electrostatic repulsion between the negatively charged HA molecules and the negatively charged HAP surface, which may cause a significantly decreased HA adsorption capacity with increasing initial pH from 8 to 12.

#### Adsorption isotherms of HA on HZC and SMHZC

The adsorption isotherms of HA on HZC and SMHZC are shown in Fig. 6. It was shown that SMHZC exhibited a much higher adsorption capacity for HA than HZC, indicating that the surface modification of HZC with CPB significantly enhances its HA adsorption capacity and thus SMHZC is more suitable as an efficient adsorbent for removing HA from aqueous solution than HZC. The Langmuir and Freundlich isotherm models were applied to analyze the equilibrium adsorption data. The Langmuir isotherm model assumes that the adsorption takes place at specific homogenous sites within the adsorbent and is commonly used for monolayer adsorption (Chen et al. 2011). The linearized form of Langmuir isotherm model can be written as (Chen et al. 2011):

$$\frac{C_e}{q_e} = \frac{C_e}{q_m} + \frac{1}{q_m K_L} \quad (3)$$

where  $q_e$  is the amount of adsorbate adsorbed per unit of adsorbent at equilibrium time (in milligrams per gram),  $C_e$  is the equilibrium concentration of adsorbate in solution (in milligrams per liter),  $q_m$  is the maximum monolayer adsorption capacity (in milligrams per gram), and  $K_L$  is the Langmuir constant related to the energy of adsorption (in liters per milligram). The values of  $q_m$  and  $K_L$  can be predicted from the slope and the intercept of the plot of  $C_e/q_e$  versus  $C_e$ . In order to determine whether the adsorption is favorable, a dimensionless constant separation factor or equilibrium parameter ( $R_L$ ) is defined based on the following equation (Venkatesha et al. 2012):

$$R_L = \frac{1}{1 + K_L C_0} \quad (4)$$

where  $C_0$  is the initial adsorbate concentration (in milligrams



**Table 1** Isotherm parameters for HA adsorption onto HZC and SMHZC

Adsorbent	Langmuir isotherm			Freundlich isotherm		
	$q_m$ (mg/g)	$K_L$ (L/mg)	$R^2$	$K_F$ (mg <sup>1-1/n</sup> L <sup>1/n</sup> /g)	1/n	$R^2$
HZC	75.8	0.0511	0.975	7.46	0.497	0.860
SMHZC	227.7	0.119	0.995	52.0	0.322	0.906

per liter). The values of  $R_L$  indicate the adsorption to be either unfavorable ( $R_L > 1$ ), linear ( $R_L = 1$ ), favorable ( $0 < R_L < 1$ ), or irreversible ( $R_L = 0$ ) (Venkatesha et al. 2012). The Freundlich isotherm model is usually used to describe the multilayer adsorption behavior for heterogeneous surfaces, and its linearized form can be written as (Tang et al. 2012; Tao et al. 2010):

$$\ln(q_e) = \ln(K_F) + \frac{1}{n} \ln(C_e) \tag{5}$$

where  $K_F$  (in mg<sup>1-1/n</sup>L<sup>1/n</sup>/g) and 1/n are isotherm constants which indicate the capacity and the intensity of the adsorption, respectively. The values of 1/n and  $K_F$  can be predicted from the slope and the intercept of the plot of  $\ln(q_e)$  versus  $\ln(C_e)$ .

The obtained parameters of Langmuir and Freundlich isotherm models for HA adsorption onto HZC and SMHZC along with correlation coefficients ( $R^2$ ) are shown in Table 1. The Langmuir isotherm model gave a much better fit to the experimental data compared to that of the Freundlich isotherm model, revealing that the adsorption of HA on HZC and SMHZC is monolayer coverage rather than multilayer adsorption. According to the Langmuir isotherm model, the predicted maximum monolayer HA adsorption

capacities for HZC and SMHZC at pH 7 were found to be 75.8 and 227.7 mg/g, respectively. It is evident that the maximum HA adsorption capacity for SMHZC was much higher than that for HZC and was also much higher than that for those adsorbents had been reported in previous literatures (as shown in Table 2). This indicates that SMHZC is a very promising adsorbent for HA removal from aqueous solution. The  $R_L$  values for HA adsorption onto HZC and SMHZC were in the range of 0.123–0.662 and 0.0360–0.251, respectively. This indicates that the adsorption of HA on HZC and SMHZC is favorable.

*Adsorption kinetics of HA on SMHZC*

The adsorption kinetics of HA on SMHZC at different initial adsorbate concentrations are shown in Fig. 7. It was shown that the amounts of HA adsorbed at different initial adsorbate concentrations increased with the increase of contact time until an equilibrium was reached. It was also shown that the amounts of HA adsorbed at different contact time increased with increasing initial adsorbate concentration. This is due to the increase in the mass driving force which allows more HA molecules to pass

**Table 2** The comparison of maximum HA adsorption capacities of various adsorbents

Adsorbent	$q_m$ (mg/g)	Reference
Acid-activated Greek bentonite	12.062	Doulia et al. 2009
Polyaniline/attapulgitite composite	61.35	Wang et al. 2011b
Palygorskite	17	Wang et al. 2011c
Modified rice husk ash	8.2	Imyim and Prapalimrungsi 2010
Activated carbon prepared from biomass material	45.4	Daifullah et al. 2004
Granular activated carbon (Filtrisorb 200)	2.51	Chen and Wu 2004
Granular activated carbon (Filtrisorb 400)	55.8	Maghsoodloo et al. 2011
Chitosan treated granular activated carbon (Filtrisorb 400)	71.4	Maghsoodloo et al. 2011
Layer structured graphite oxide	190	Hartono et al. 2009
Aminopropyl functionalized SBA-15	117.6	Tao et al. 2010
Mg/Fe layered double hydroxide	76.70	Gasser et al. 2008
PEI functionalized magnetic mesoporous silica composite microspheres (MS-PEI)	128.64	Tang et al. 2012
Bi-functional resin JN-10	105.31	Wang et al. 2010
CPB-modified zeolite	92.0	Zhan et al. 2010
HTAB-modified zeolite synthesized from coal fly ash	126.6	Li et al. 2011
SMHZC	227.7	This study



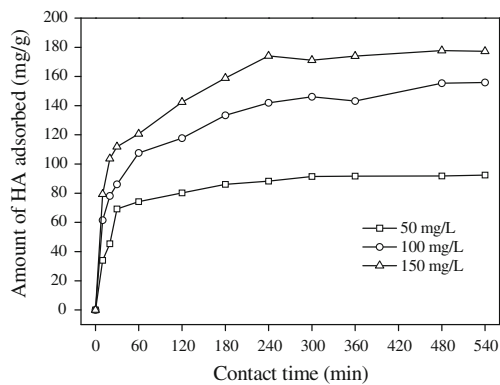


**Fig. 7** Adsorption kinetics of HA on SMHZC at various initial adsorbate concentrations (solution volume 50 mL; pH 7; adsorbent dosage 0.5 g/L; temperature 303 K)

from the solution to the surface of the adsorbent (Doulia et al. 2009). In order to investigate the mechanism of HA adsorption onto SMHZC, three widely used kinetic models, namely pseudo-first-order, pseudo-second-order, and intra-particle diffusion models, were applied to analyze the kinetic data. The linearized form of pseudo-first-order kinetic model can be written as (Doulia et al. 2009):

$$\ln(q_e - q_t) = \ln(q_e) - k_1 t \quad (6)$$

where  $q_t$  and  $q_e$  are the amounts of adsorbate adsorbed (in milligrams per gram) at any time  $t$  and at equilibrium time, respectively.  $k_1$  is the pseudo-first-order adsorption rate constant (1/min). The values of  $k_1$  and  $q_e$  can be calculated from the linear plot of  $\ln(q_e - q_t)$  versus  $t$ . The linearized form of pseudo-second-order kinetic model can be written as (Doulia et al. 2009):

$$\frac{t}{q_t} = \frac{t}{q_e} + \frac{1}{k_2 q_e^2} \quad (7)$$

where  $k_2$  is the pseudo-second-order adsorption rate constant (in grams per milligram minute). The values of  $k_2$  and  $q_e$  can be calculated from the linear plot of  $t/q_t$  versus  $t$ . The obtained parameters of pseudo-first-order and pseudo-second-order kinetic models along with correlation coefficients ( $R^2$ ) are shown in Table 3. Although the correlation coefficient value for the pseudo-first-order kinetic model was relatively high or high, the calculated  $q_e$  value was not in agreement with the experimental one. Therefore, the adsorption of HA on SMHZC does not

follow the pseudo-first-order kinetic model. The correlation coefficient value for the pseudo-second-order kinetic model was very high, and the calculated  $q_e$  value was in good agreement with the experimental one. Therefore, the adsorption of HA on SMHZC follows the pseudo-second-order kinetic model.

The mechanisms for HA adsorption onto SMHZC may consist of four steps: transport of HA molecules from the bulk solution to the adsorbent surface, diffusion through the boundary layer to the adsorbent surface, adsorption at sites on the adsorbent surface, and intra-particle diffusion into the adsorbent pore. Generally, bulk transport and adsorption at sites on the adsorbent surface are rapid processes, while diffusions including film diffusion (boundary layer diffusion) and intra-particle diffusion are slow processes and thus rate-limiting steps (Bia et al. 2012). The intra-particle diffusion model proposed by Weber and Morris were used to identify whether the intra-particle diffusion process is a rate-limiting step in the adsorption process of HA on SMHZC. The linearized form of intra-particle diffusion model can be written as (Bia et al. 2012):

$$q_t = k_i t^{1/2} + C \quad (8)$$

where  $k_i$  is the intra-particle diffusion rate constant (in mg/g min<sup>1/2</sup>) and  $C$  is the intercept (in milligrams per gram), related to the thickness of the boundary layer. According to this model, if the intra-particle diffusion is the sole rate-limiting step, a plot of  $q_t$  versus  $t^{1/2}$  is a straight line passing through the origin (Bia et al. 2012). Otherwise, both film and intra-particle diffusion processes are the rate-limiting steps (Bia et al. 2012). The plots of  $q_t$  versus  $t^{1/2}$  for HA adsorption onto SMHZC at different initial adsorbate concentrations are shown in Fig. 8. It was shown that the adsorption process includes three different stages: (a) the first sharper portion being a fast external surface adsorption stage, (b) the second linear portion being a gradual adsorption stage where intra-particle diffusion was rate-limited, and (c) the third portion being a final equilibrium stage where intra-particle diffusion started to slow down. As the second portion of the plot of  $q_t$  versus  $t^{1/2}$  did not pass through the origin (Fig. 8), the intra-particle diffusion was not the sole rate-limiting step during the gradual adsorption stage, and both film and intra-particle diffusions took place simultaneously.

**Table 3** Kinetic model rate constants for HA adsorption on SMHZC

$C_0$ (mg/L)	$q_{e,exp}$ (mg/g)	Pseudo-first-order model			Pseudo-second-order model		
		$q_{e,cal}$ (mg/g)	$k_1$ (1/min)	$R^2$	$q_{e,cal}$ (mg/g)	$k_2$ (g/mgmin)	$R^2$
50	92.4	45.5	0.0106	0.926	95.2	0.000580	1.00
100	155.8	94.6	0.00757	0.989	161.6	0.000208	0.997
150	177.8	95.1	0.00881	0.979	184.8	0.000239	0.999

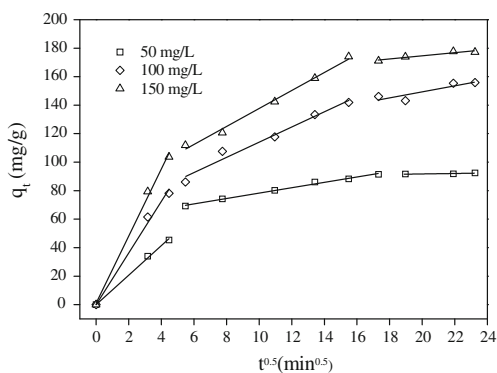


**Fig. 8** Plot of  $q_t$  versus  $t^{0.5}$  for HA adsorption onto SMHZC

*Effect of coexisting Cu(II) on HA adsorption onto SMHZC*

The adsorption of HA on SMHZC as a function of coexisting Cu(II) is shown in Fig. 9. The presence of Cu(II) in solution led to markedly enhanced HA adsorption onto SMHZC. This may be explained as follows: Coexisting Cu(II) ions tend to form complexes with carboxyl and phenolic groups of HA molecules to produce intermolecular bonds between HA molecules, which may result in that more HA molecules are adsorbed by the same amounts of the adsorption sites on the surface of SMHZC. In addition, coexisting Cu(II) in solution may neutralize the repulsive force between HA molecules in solution and HA molecules adsorbed on the surface of the adsorbent, which may favor the adsorption of HA onto SMHZC.

Adsorption of Cu(II) on SMHZC

*Effect of adsorbent dosage on Cu(II) adsorption onto SMHZC*

The adsorption of Cu(II) on SMHZC as a function of adsorbent dosage is shown in Fig. 10. It was shown that the Cu(II) removal efficiency of SMHZC increased from 52 to

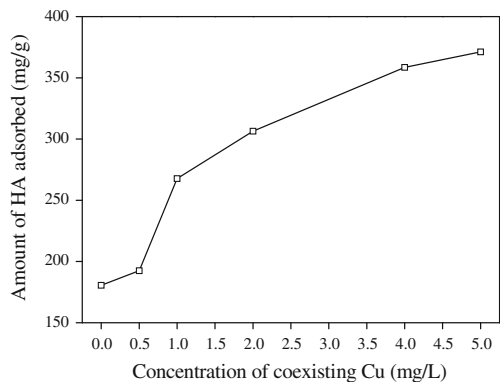


**Fig. 9** Effect of coexisting Cu(II) on HA adsorption onto SMHZC (solution volume 200 mL; pH 6; adsorbent dosage 0.05 g/L; initial HA concentration 20 mg/L; temperature 303 K; contact time 24 h)

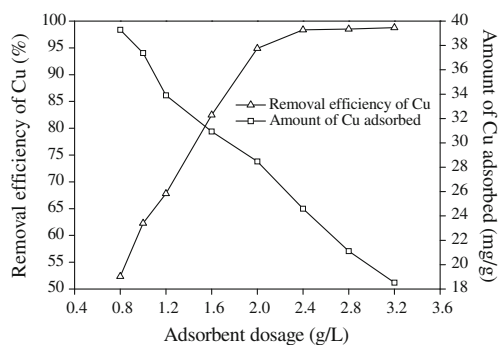


**Fig. 10** Effect of adsorbent dosage on Cu(II) adsorption onto SMHZC (solution volume 25 mL; initial Cu(II) concentration 60 mg/L; pH 6; contact time 24 h; temperature 303 K)

98 % with the increase of adsorbent dosage from 0.8 to 2.4 g/L. With a further increase in the dosage of SMHZC to 3.2 g/L, the Cu(II) removal efficiency slightly went up to 99 %. However, the amount of Cu(II) adsorbed onto SMHZC decreased significantly with the increase of adsorbent dosage from 0.2 to 3.2 g/L. Similar trend has been observed for HA adsorption onto SMHZC.

*Effect of solution pH on Cu(II) adsorption onto SMHZC*

The adsorption of Cu(II) on SMHZC as a function of solution pH is shown in Fig. 11. It was shown that the Cu(II) adsorption capacity for SMHZC increased with the increase of initial pH from 3 to 6.5 and remained unchanged with the increase of initial pH from 6.5 to 7.5. This indicates that the Cu(II) adsorption capacity for SMHZC in weakly acidic or neutral solution is better than that in strongly acidic solution. It is well-known that the ion exchange between the exchangeable inorganic cations within the zeolite crystal structure and Cu(II) ions is an important mechanism that governs the adsorption of Cu(II) on zeolite (Motsi et al. 2009; Šljivić et al. 2009a). The CPB molecules are too large to enter into the internal zeolite channels and the loading of CPB

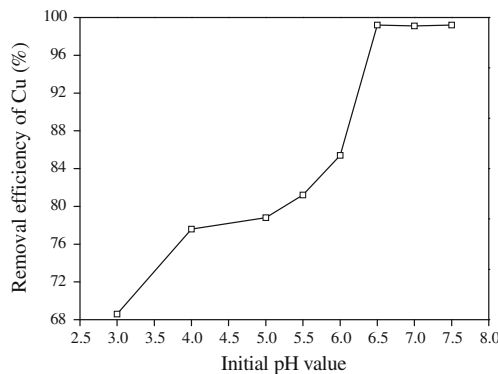


**Fig. 11** Effect of solution pH on Cu(II) adsorption onto SMHZC (solution volume 25 mL; initial Cu(II) concentration 60 mg/L; adsorbent dosage 1.6 g/L; contact time 24 h; temperature 303 K)

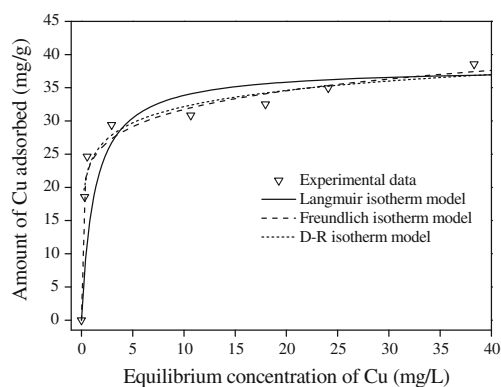


**Fig. 12** Adsorption isotherm of Cu(II) on SMHZC (solution volume 25 mL; pH 6; adsorbent dosage 1.6 g/L; contact time 24 h; temperature 303 K)

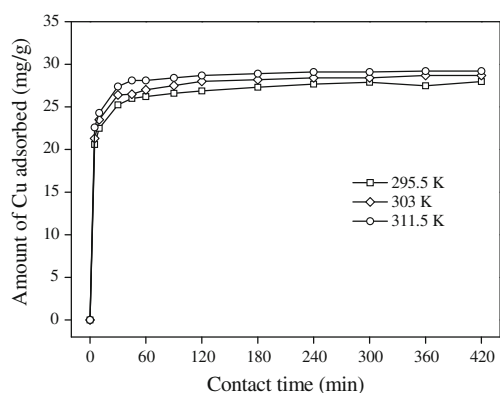


**Fig. 13** Adsorption kinetics of Cu(II) on SMHZC at various temperatures (solution volume 25 mL; initial Cu(II) concentration 60 mg/L; pH 6; adsorbent dosage 2 g/L)

molecules on zeolite is only restricted to the external cation exchange sites (Li et al. 2000; Zhan et al. 2010). Therefore, we deduce that the ion exchange with the exchangeable inorganic cations within the internal zeolite channels is an important mechanism that governs the adsorption of Cu(II) on SMHZC. There are three possible mechanisms that govern the removal of Cu(II) from aqueous solution by HAP (Corami et al. 2008; Šljivić et al. 2009b; Wang et al. 2009). The first mechanism is the surface complexation of Cu(II) on the  $\equiv\text{P}-\text{OH}$  groups of HAP (Corami et al. 2008; Wang et al. 2009). The second mechanism is the ion exchange with  $\text{Ca}^{2+}$  of HAP (Corami et al. 2008; Wang et al. 2009; Šljivić et al. 2009b). The third mechanism is the dissolution of HAP followed by the precipitation of copper-containing hydroxyapatite with formula  $\text{Cu}_x\text{Ca}_{10-x}(\text{PO}_4)_6(\text{OH})_2$  (Corami et al. 2008; Šljivić et al. 2009b). Therefore, we deduce that the mechanisms for the adsorption of Cu(II) on SMHZC may include the surface complexation of the  $\equiv\text{P}-\text{OH}$  groups of HAP, the ion exchange with  $\text{Ca}^{2+}$  of HAP, and the dissolution of HAP followed by the precipitation of copper-containing hydroxyapatite. The drop in equilibrium pH suggests that  $\text{H}^+$  ions are liberated from the HAP surface into the aqueous phase as a result of the exchange with heavy metal ions (Corami et al. 2008; Smičiklas et al. 2006). The observed pH decreases after Cu(II) adsorption at initial pH 5.5–6 confirm that the surface complexation is an important mechanism for Cu(II) adsorption onto SMHZC. The increase in the Cu(II) adsorption capacity for SMHZC with the increase of initial pH from 3 to 6.5 may be explained on the basis of proton-competitive

adsorption reactions. At lower pH value, more hydrogen ions compete with Cu(II) ions for the surface binding sites of SMHZC, thereby causing a lower Cu(II) adsorption capacity. As the solution pH increases, the concentration of the hydrogen ions as competitors decreases and this causes an increase in the Cu(II) adsorption capacity. The amount of metal hydroxide increases with the increase of solution pH, which also intensifies the adsorption of Cu(II) via precipitation mechanism (Wang et al. 2008).

#### Adsorption isotherm of Cu(II) on SMHZC

The adsorption isotherm of Cu(II) on SMHZC is shown in Fig. 12. It was shown that the Cu(II) adsorption capacity for SMHZC increased with the increase of the equilibrium Cu(II) concentration. The Langmuir and Freundlich isotherm models were applied to analyze the equilibrium adsorption data. The obtained parameters of Langmuir and Freundlich isotherm models for Cu(II) adsorption onto SMHZC along with correlation coefficients ( $R^2$ ) are shown in Table 4. It was shown that the equilibrium adsorption data of Cu(II) on SMHZC could be described by the Langmuir and Freundlich isotherm models. According to the Langmuir isotherm model, the predicted maximum Cu(II) monolayer adsorption capacity for SMHZC at pH 6 was found to be 38.1 mg/g under our experimental condition, which is much higher than that of natural zeolite reported in previous literatures (3.37–23.3 mg/g) (Motsi et al. 2009; Šljivić et al. 2009a; Wang et al. 2008). This indicates that SMHZC is

**Table 4** Isotherm parameters for Cu(II) adsorption onto SMHZC

Langmuir isotherm			Freundlich isotherm			D-R isotherm			
$q_m$ (mg/g)	$K_L$ (L/mg)	$R^2$	$K_F$ ( $\text{mg}^{1-1/n}\text{L}^{1/n}/\text{g}$ )	$1/n$	$R^2$	$q_0$ (mmol/g)	$K_D$ ( $\text{mol}^2/\text{kJ}^2$ )	$E$ (kJ/mol)	$R^2$
38.1	0.796	0.991	23.9	0.123	0.911	0.813	0.000987	22.5	0.920

**Table 5** Kinetic model rate constants for Cu(II) adsorption onto SMHZC

T (K)	$q_{e,exp}$ (mg/g)	Pseudo-first-order model			Pseudo-second-order model		
		$q_{e,cal}$ (mg/g)	$k_1$ (1/min)	$R^2$	$q_{e,cal}$ (mg/g)	$k_2$ (g/mgmin)	$R^2$
295.5	28.0	4.90	0.0124	0.866	28.0	0.00996	1.00
303	28.7	5.85	0.0191	0.926	28.8	0.0105	1.00
311.5	29.2	3.59	0.0134	0.873	29.3	0.0143	1.00

more suitable as an efficient adsorbent for Cu(II) removal from aqueous solution than natural zeolite. The  $R_L$  values for Cu(II) adsorption onto SMHZC were in the range of 0.0124–0.0402. This indicates that the adsorption of Cu(II) on SMHZC is favorable.

In order to determine the nature of the adsorption process as physical or chemical, the Dubinin–Radushkevich (D–R) isotherm model was also applied to analyze the equilibrium adsorption data. The linearized form of D–R isotherm model can be written as (Chen et al. 2011):

$$\ln(q_e) = \ln(q_0) - K_D \varepsilon^2 \tag{9}$$

where  $q_e$  is the amount of adsorbate adsorbed per unit of adsorbent at equilibrium time (in moles per gram),  $q_0$  is the maximum adsorption capacity (in moles per gram),  $K_D$  is the isotherm constant related to the adsorption energy (in square moles per square kilojoule),  $\varepsilon$  is the Polanyi potential and equal to  $RT \ln(1+1/C_e)$ ,  $R$  is the universal gas constant (8.314 J/molK),  $T$  is the temperature (kelvin), and  $C_e$  is the equilibrium concentration of adsorbate in solution (in moles per liter). The values of  $K_D$  and  $q_0$  can be predicted from the slope and the intercept of the plot of  $\ln(q_e)$  versus  $\varepsilon^2$ . The obtained parameters of D–R isotherm model for Cu(II) adsorption onto SMHZC along with correlation coefficient ( $R^2$ ) are shown in Table 4. It was shown that the equilibrium adsorption data of Cu(II) on SMHZC could be described by the D–R isotherm model. The value of mean free energy of adsorption ( $E$ , in kilojoules per mole) can

be calculated as follows (Chen et al. 2011):

$$E = (2K_D)^{-0.5} \tag{10}$$

It is well-known that the magnitude of  $E$  is useful for estimating the type of adsorption, and if this value is below 8 kJ/mol, the adsorption type can be explained by physical adsorption (Chen et al. 2011). If the value of  $E$  is between 8 and 16 kJ/mol, the adsorption type can be explained by ion exchange, and if the value of  $E$  is between 20 and 40 kJ/mol, the adsorption type can be explained by chemical adsorption (Chen et al. 2011). The value of  $E$  obtained from the present study was between 20 and 40 kJ/mol, indicating that the adsorption of Cu(II) on SMHZC involves a chemical adsorption mechanism. This confirms that the mechanisms for the adsorption of Cu(II) on SMHZC include surface complexation and dissolution-precipitation.

*Adsorption kinetics of Cu(II) on SMHZC*

The adsorption kinetics of Cu(II) on SMHZC at different temperatures are shown in Fig. 13. It was shown that the amounts of Cu(II) adsorbed at different temperatures increased with the increase of contact time until an equilibrium was reached. It was also shown that the amounts of Cu (II) adsorbed at different contact time increased with increasing temperature, indicating an overall endothermic process. In order to investigate the mechanism of Cu(II)

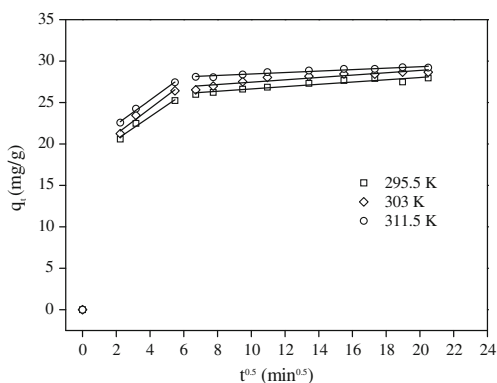


**Fig. 14** Plot of  $q_t$  versus  $t^{0.5}$  for Cu(II) adsorption onto SMHZC

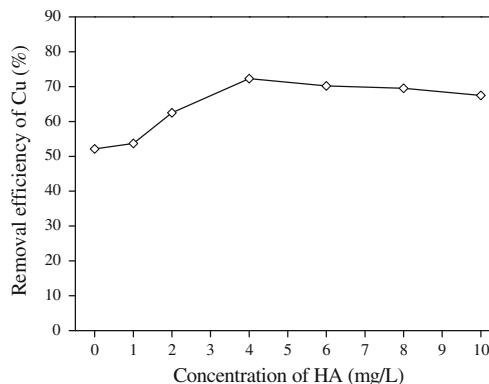


**Fig. 15** Effect of coexisting HA on Cu(II) adsorption onto SMHZC (solution volume 200 mL; pH 6; adsorbent dosage 0.05 g/L; initial Cu (II) concentration 5 mg/L; temperature 303 K; contact time 24 h)



adsorption onto SMHZC, three widely used kinetic models, namely pseudo-first-order, pseudo-second-order, and intra-particle diffusion models, were applied to analyze the kinetic data. The obtained results are shown in Table 5 and Fig. 14. As shown in Table 5, the adsorption of Cu(II) on SMHZC does not follow the pseudo-first-order kinetic model, but follows the pseudo-second-order kinetic model. As shown in Fig. 14, the adsorption of Cu(II) on SMHZC takes place in three different stages: fast external surface adsorption, gradual adsorption controlled by both film and intra-particle diffusions, and final equilibrium stage.

#### *Effect of coexisting HA on Cu(II) adsorption onto SMHZC*

In theory, HA may influence the adsorption of Cu(II) on SMHZC in three ways. First, the adsorption of HA may increase the negative charge on the SMHZC surface, thereby increasing Cu(II) adsorption; second, by competing with the adsorption sites of SMHZC for Cu(II), the presence of HA may decrease Cu(II) adsorption; third, HA reacts with Cu(II) to form HA–Cu(II) complexes, which influence Cu(II) speciation and its adsorption onto SMHZC (Wang et al. 2008, 2009). In the present study, the effect of coexisting HA on Cu(II) adsorption onto SMHZC was investigated, and the obtained results are shown in Fig. 15. It was shown that the Cu(II) removal efficiency in the presence of HA was higher than that in the absence of HA, indicating that coexisting HA enhances Cu(II) adsorption onto SMHZC. Similar influence of coexisting HA on Cu(II) adsorption was observed for activated carbon (Terdkiatburana et al. 2008). This may be attributed to two reasons. The adsorption of HA on SMHZC can cause an increase in the surface negative charges, which may favor Cu(II) adsorption. HA and Cu(II) can form complexes in solution, and HA–Cu(II) complexes can be easily adsorbed on the adsorption sites of SMHZC for HA, which also may favor Cu(II) adsorption.

#### **Conclusion**

SMHZC exhibited much higher HA adsorption capacity than HZC. The HA adsorption capacity for SMHZC decreased slightly with increasing pH from 3 to 8 but decreased significantly with increasing pH from 8 to 12. The Cu(II) adsorption capacity for SMHZC increased with increasing pH from 3 to 6.5. The adsorption of HA and Cu(II) on SMHZC obeyed a pseudo-second-order kinetic model. The adsorption of HA and Cu(II) on SMHZC took place in three different stages: fast external surface adsorption, gradual adsorption controlled by both film and intra-particle diffusions, and final equilibrium stage. The equilibrium adsorption data of HA on SMHZC better fitted to the Langmuir isotherm model than the Freundlich isotherm

model. According to the Langmuir isotherm model, the predicted maximum HA monolayer adsorption capacity for SMHZC was found to be 227.7 mg/g at pH 7. The equilibrium adsorption data of Cu(II) on SMHZC could be described by the Langmuir, Freundlich, and D–R isotherm models. The presence of Cu(II) in solution enhanced HA adsorption onto SMHZC. The presence of HA in solution enhanced Cu(II) adsorption onto SMHZC. The adsorption of HA on SMHZC at pH 7 may be achieved via electrostatic attraction, organic partitioning, hydrogen bonding, and Lewis acid–base interaction. The adsorption of Cu(II) on SMHZC at pH 6 may be achieved via surface complexation, ion exchange, and dissolution–precipitation. Results of this work indicate that SMHZC can be used as an effective adsorbent to simultaneously remove HA and Cu(II) from water.

**Acknowledgments** This work was supported by the National Natural Science Foundation of China (50908142); the Foundation of Key Laboratory of Yangtze River Water Environment, Ministry of Education (Tongji University), China, (YRWEF201107); the Scientific Research Project of Shanghai Science and Technology Committee (10230502900); the Startup Foundation for Doctors of Shanghai Ocean University (B-5301-11-0219); and the Leading Academic Discipline Project of Shanghai Municipal Education Commission (J50702). We also thank the editors and the anonymous reviewers whose comments and suggestions greatly improved the quality of this manuscript.

#### **References**

- Balistreri LS, Murray JW (1981) The surface chemistry of goethite ( $\alpha$ -FeOOH) in major ion seawater. *Am J Sci* 281:788–806
- Bia G, Pauli CPD, Borgnino L (2012) The role of Fe(III) modified montmorillonite on fluoride mobility: adsorption experiments and competition with phosphate. *J Environ Manag* 100:1–9
- Bouhamed F, Elouear Z, Bouzid J (2012) Adsorptive removal of copper(II) from aqueous solutions on activated carbon prepared from Tunisian date stones: equilibrium, kinetics and thermodynamics. *J Taiwan Inst Chem Eng*. doi:10.1016/j.jtice.2012.02.011
- Bouyarmane H, Asri SE, Rami A, Roux C, Mahly MA, Saoiabi A, Coradinc T, Laghzizil A (2010) Pyridine and phenol removal using natural and synthetic apatites as low cost sorbents: influence of porosity and surface interactions. *J Hazard Mater* 181:736–741
- Chao HP, Chen SH (2012) Adsorption characteristics of both cationic and oxyanionic metal ions on hexadecyltrimethylammonium bromide-modified NaY zeolite. *Chem Eng J* 193–194:283–289
- Chen JP, Wu SN (2004) Simultaneous adsorption of copper ions and humic acid onto an activated carbon. *J Colloid Interf Sci* 280:334–342
- Chen H, Zhao J, Wu JY, Dai GL (2011) Isotherm, thermodynamic, kinetics and adsorption mechanism studies of methyl orange by surfactant modified silkworm exuviae. *J Hazard Mater* 192:246–254
- Corami A, Mignardi S, Ferrini V (2007) Copper and zinc decontamination from single- and binary-metal solutions using hydroxyapatite. *J Hazard Mater* 146:164–170
- Corami A, Mignardi S, Ferrini V (2008) Cadmium removal from single- and multi-metal (Cd+Pb+Zn+Cu) solutions by sorption on hydroxyapatite. *J Colloid Interf Sci* 317:402–408

- Da'na E, Sayari A (2011) Optimization of copper removal efficiency by adsorption on amine-modified SBA-15: experimental design methodology. *Chem Eng J* 167:91–98
- Daifullah AAM, Girgis BS, Gad HMH (2004) A study of the factors affecting the removal of humic acid by activated carbon prepared from biomass material. *Colloid Surface A* 235:1–10
- Demirbas E, Dizge N, Sulak MT, Kobya M (2009) Adsorption kinetics and equilibrium of copper from aqueous solutions using hazelnut shell activated carbon. *Chem Eng J* 148:480–487
- Ding CL, Shang C (2010) Mechanisms controlling adsorption of natural organic matter on surfactant-modified iron oxide-coated sand. *Water Res* 44:3651–3658
- Douliou D, Leodopoulos C, Gimouhopoulos K, Rigas F (2009) Adsorption of humic acid on acid-activated Greek bentonite. *J Colloid Interf Sci* 340:131–141
- Elaiopoulos K, Perraki T, Grigoropoulou E (2010) Monitoring the effect of hydrothermal treatments on the structure of a natural zeolite through a combined XRD, FTIR, XRF, SEM and N<sub>2</sub>-porosimetry analysis. *Microporous Mesoporous Mater* 134:29–43
- Elkady MF, Mahmoud MM, Abd-El-Rahman HM (2011) Kinetic approach for cadmium sorption using microwave synthesized nano-hydroxyapatite. *J Non-Cryst Solids* 357:1118–1129
- Engates KE, Shipley HJ (2011) Adsorption of Pb, Cd, Cu, Zn, and Ni to titanium dioxide nanoparticles: effect of particle size, solid concentration, and exhaustion. *Environ Sci Pollut Res* 18:386–395
- Gasser MS, Mohsen HT, Aly HF (2008) Humic acid adsorption onto Mg/Fe layered double hydroxide. *Colloid Surface A* 331:195–201
- Guan HD, Bestland E, Zhu CY, Zhu HL, Albertsdottir D, Hutson J, Simmons CT, Ginic-Markovic M, Tao X, Ellis AV (2010) Variation in performance of surfactant loading and resulting nitrate removal among four selected natural zeolites. *J Hazard Mater* 183:616–621
- Hartono T, Wang SB, Ma Q, Zhu ZH (2009) Layer structured graphite oxide as a novel adsorbent for humic acid removal from aqueous solution. *J Colloid Interf Sci* 333:114–119
- Hasret E, Ipekoglu M, Altintas S, Ipekoglu NA (2012) Microwave-assisted synthesis of hydroxyapatite for the removal of lead(II) from aqueous solutions. *Environ Sci Pollut Res* 19:2766–2775
- Imyim A, Prapalimrunsi E (2010) Humic acids removal from water by aminopropyl functionalized rice husk ash. *J Hazard Mater* 184:775–781
- Jamil TS, Ibrahim HS, Abd El-Maksoud IH, El-Wakeel ST (2010) Application of zeolite prepared from Egyptian kaolin for removal of heavy metals: I. Optimum conditions. *Desalination* 258:34–40
- Jarvis KL, Majewski P (2012) Plasma polymerized allylamine coated quartz particles for humic acid removal. *J Colloid Interf Sci* 380:150–158
- Lee SM, Laldawngliana C, Tiwari D (2012) Iron oxide nano-particles-immobilized-sand material in the treatment of Cu(II), Cd(II) and Pb(II) contaminated waste waters. *Chem Eng J* 195–196:103–111
- Li ZH, Burt T, Bowman RS (2000) Sorption of ionizable organic solutes by surfactant-modified zeolite. *Environ Sci Technol* 34:3756–3760
- Li CJ, Dong Y, Wu DY, Peng LC, Kong HN (2011) Surfactant modified zeolite as adsorbent for removal of humic acid from water. *Appl Clay Sci* 52:353–357
- Maghsoodloo S, Noroozi B, Haghi AK, Sorial GA (2011) Consequence of chitosan treating on the adsorption of humic acid by granular activated carbon. *J Hazard Mater* 191:380–387
- Malekian R, Abedi-Koupai J, Eslamian SS (2011) Influences of clinoptilolite and surfactant-modified clinoptilolite zeolite on nitrate leaching and plant growth. *J Hazard Mater* 185:970–976
- Meski S, Ziani S, Khireddine H, Boudboub S, Zaidi S (2011) Factorial design analysis for sorption of zinc on hydroxyapatite. *J Hazard Mater* 186:1007–1017
- Motsi T, Rowson NA, Simmons MJH (2009) Adsorption of heavy metals from acid mine drainage by natural zeolite. *Int J Miner Process* 92:42–48
- Motsi T, Rowson NA, Simmons MJH (2011) Kinetic studies of the removal of heavy metals from acid mine drainage by natural zeolite. *Int J Miner Process* 101:42–49
- Moussavi G, Talebi S, Farrokhi M, Sabouti RM (2011) The investigation of mechanism, kinetic and isotherm of ammonia and humic acid co-adsorption onto natural zeolite. *Chem Eng J* 171:1159–1169
- Neupane G, Donahoe RJ (2012) Attenuation of trace elements in coal fly ash leachates by surfactant-modified zeolite. *J Hazard Mater* 229–230:201–208
- Rauthula MS, Srivastava VC (2011) Studies on adsorption/desorption of nitrobenzene and humic acid onto/from activated carbon. *Chem Eng J* 168:35–43
- Shaltout AA, Allam MA, Moharram MA (2011) FTIR spectroscopic, thermal and XRD characterization of hydroxyapatite from new natural sources. *Spectrochim Acta A* 83:56–60
- Šljivić M, Smičiklas I, Pejanović S, Plečaš I (2009a) Comparative study of Cu<sup>2+</sup> adsorption on a zeolite, a clay and a diatomite from Serbia. *Appl Clay Sci* 43:33–40
- Šljivić M, Smičiklas I, Plečaš I, Mitrić M (2009b) The influence of equilibration conditions and hydroxyapatite physico-chemical properties onto retention of Cu<sup>2+</sup> ion. *Chem Eng J* 148:80–88
- Smičiklas ID, Milonjić SK, Pfendt P, Raičević S (2000) The point of zero charge and sorption of cadmium (II) and strontium (II) ions on synthetic hydroxyapatite. *Sep Purif Technol* 18:185–194
- Smičiklas I, Dimović S, Plečaš I, Mitrić M (2006) Removal of Co<sup>2+</sup> from aqueous solutions by hydroxyapatite. *Water Res* 40:2267–2274
- Stárek J, Zukal A, Rathouský J (1994) Comparison of the adsorption of humic acids from aqueous solutions on active carbon and activated charcoal cloths. *Carbon* 32:207–211
- Sulaymon AH, Ebrahim SE, Mohammed-Ridha MJ (2012) Equilibrium, kinetic, and thermodynamic biosorption of Pb(II), Cr(III), and Cd(II) ions by dead anaerobic biomass from synthetic wastewater. *Environ Sci Pollut Res*. doi:10.1007/s11356-012-0854-8
- Suresh Kumar G, Girija EK, Thamizhavel A, Yokogawa Y, Narayana Kalkura S (2010) Synthesis and characterization of bioactive hydroxyapatite-calcite nanocomposite for biomedical applications. *J Colloid Interf Sci* 349:56–62
- Tanaka H, Watanabe T, Chikazawa M (1997) FTIR and TPD studies on the adsorption of pyridine, *n*-butylamine and acetic acid on calcium hydroxyapatite. *J Chem Soc, Faraday Trans* 93:4377–4381
- Tang YL, Liang S, Yu SL, Gao NY, Zhang J, Guo HC, Wang YL (2012) Enhanced adsorption of humic acid on amine functionalized magnetic mesoporous composite microspheres. *Colloid Surface A* 406:61–67
- Tao Q, Xu ZY, Wang JH, Liu FL, Wan HQ, Zheng SR (2010) Adsorption of humic acid to aminopropyl functionalized SBA-15. *Microporous Mesoporous Mater* 131:177–185
- Terdkiatburana T, Wang SB, Tadé MO (2008) Competition and complexation of heavy metal ions and humic acid on zeolitic MCM-22 and activated carbon. *Chem Eng J* 139:437–444
- Tong KS, Jain Kassim M, Azraa A (2011) Adsorption of copper ion from its aqueous solution by a novel biosorbent *Uncaria gambir*: equilibrium, kinetics, and thermodynamic studies. *Chem Eng J* 170:145–153
- Venkatesha TG, Viswanatha R, Arthoba Nayaka Y, Chethana BK (2012) Kinetics and thermodynamics of reactive and vat dyes adsorption on MgO nanoparticles. *Chem Eng J* 198–199:1–10
- Wang SB, Ariyanto E (2007) Competitive adsorption of malachite green and Pb ions on natural zeolite. *J Colloid Interf Sci* 314:25–31

- Wang SG, Gong WX, Liu XW, Gao BY, Yue QY (2006) Removal of fulvic acids using the surfactant modified zeolite in a fixed-bed reactor. *Sep Purif Technol* 51:367–373
- Wang SB, Terdkiatburana T, Tadé MO (2008) Adsorption of Cu(II), Pb (II) and humic acid on natural zeolite tuff in single and binary systems. *Sep Purif Technol* 62:64–70
- Wang YJ, Chen JH, Cui YX, Wang SQ, Zhou DM (2009) Effects of low-molecular-weight organic acids on Cu(II) adsorption onto hydroxyapatite nanoparticles. *J Hazard Mater* 162:1135–1140
- Wang JN, Zhou Y, Li AM, Xu L (2010) Adsorption of humic acid by bi-functional resin JN-10 and the effect of alkali-earth metal ions on the adsorption. *J Hazard Mater* 176:1018–1026
- Wang XJ, Liang X, Wang Y, Wang X, Liu M, Yin DQ, Xia SQ, Zhao JF, Zhang YL (2011a) Adsorption of Copper (II) onto activated carbons from sewage sludge by microwave-induced phosphoric acid and zinc chloride activation. *Desalination* 278:231–237
- Wang JH, Han XJ, Ma HR, Ji YF, Bi LJ (2011b) Adsorptive removal of humic acid from aqueous solution on polyaniline/attapulgitite composite. *Chem Eng J* 173:171–177
- Wang MS, Liao LB, Zhang XL, Li ZH (2011c) Adsorption of low concentration humic acid from water by palygorskite. *Appl Clay Sci*. doi:10.1016/j.clay.2011.09.012
- Wei W, Zhang X, Cui J, Wei ZG (2011) Interaction between low molecular weight organic acids and hydroxyapatite. *Colloid Surface A* 392(1):67–75
- Wen QX, Chen ZQ, Lian JX, Feng YJ, Ren NQ (2012) Removal of nitrobenzene from aqueous solution by a novel lipid adsorption material (LAM). *J Hazard Mater* 209–210:226–232
- Wu LM, Forsling W, Schindler PW (1991) Surface complexation of calcium minerals in aqueous solutions. 1. Surface protonation of fluoroapatite water interfaces. *J Colloid Interf Sci* 147:178–185
- Wu YH, Wen YJ, Zhou JX, Cao JL, Jin YP, Wu YY (2012) Comparative and competitive adsorption of Cr(VI), As(III), and Ni(II) onto coconut charcoal. *Environ Sci Pollut Res*. doi:10.1007/s11356-012-1066-y
- Yadav S, Srivastava V, Banerjee S, Gode F, Sharma YC (2012) Studies on the removal of nickel from aqueous solutions using modified river-bed sand. *Environ Sci Pollut Res*. doi:10.1007/s11356-012-0892-2
- Zhan YH, Zhu ZL, Lin JW, Qiu YL, Zhao JF (2010) Removal of humic acid from aqueous solution by cetylpyridinium bromide modified zeolite. *J Environ Sci* 22:1327–1334
- Zhu RH, Yu RB, Yao JX, Mao D, Xing CJ, Wang D (2008) Removal of Cd<sup>2+</sup> from aqueous solutions by hydroxyapatite. *Catal Today* 139:94–99